

Chaotic and regular motion around generalized Kalnajcs discs

Javier Ramos-Caro^{*}, Framsol López-Suspe[†] and Guillermo A. González[‡]

Escuela de Física, Grupo de Investigación en Relatividad y Gravitación, Universidad Industrial de Santander, A. A. 678, Bucaramanga, Santander, Colombia

13 November 2021

ABSTRACT

The motion of test particles in the gravitational fields generated by the first four members of the infinite family of generalized Kalnajcs discs (González & Reina (2006)), is studied. In first instance, we analyze the stability of circular orbits under radial and vertical perturbations and describe the behavior of general equatorial orbits and so we find that radial stability and vertical instability dominate such disc models. Then we study bounded axially symmetric orbits by using the Poincaré surfaces of section and Lyapunov characteristic numbers and find chaos in the case of disc-crossing orbits and completely regular motion in other cases.

Key words: stellar dynamics – galaxies: kinematics and dynamics – chaotic dynamics.

1 INTRODUCTION

A fact usually assumed in astrophysics is that the main part of the mass of a typical spiral galaxy is concentrated in a thin disk (Binney & Tremaine (1987)). Accordingly, the study of the gravitational potential generated by an idealized thin disk is a problem of great astrophysical relevance and so, through the years, different approaches has been used to obtain such kind of thin disk models(see Kuzmin (1956) and Toomre (1963; 1964), as examples). A simple method to obtain the surface density, the gravitational potential and the rotation curve of thin disks of finite radius was developed by Hunter (1963), the simplest example of disk obtained by this method being the Kalnajcs disk (Kalnajcs (1972)), which can also be obtained by flattening a uniformly rotating spheroid (Wyse & Mayall (1942); Brandt (1960); Brandt & Belton (1962)). In a previous paper (González & Reina (2006)) we use the Hunter method in order to obtain an infinite family of thin disks of finite radius, an infinite family of generalized Kalnajcs discs with a well behaved surface mass density.

Closely related with the above study is the analysis of the motion of test particles in the gravitational field generated by such disklike distributions of matter. In particular, the study of orbits in the equatorial plane is of clear astrophysical relevance due to its relation with the dynamics of intergalactic stellar motion or the flow of particles in accretion disks around black holes. Also, a knowledge of the disc's

internal kinematics is relevant for its subsequent statistical analysis, and the study of external particles motion help us to understand the behavior of stars belonging to the galaxy's remaining component (for example, the halo). Many of them cross back and forth through the disc, experiencing a fairly abrupt change in the gravitational force field. This fact gives rise to a large variety of chaotic and regular orbits, as it was pointed out by Hunter (2005), in the case of Kuzmin-like discs, and Martinet et al (1971; 1973; 1974; 1975), in the case of Schmidt's models (Schmidt 1956).

In agreement with the above considerations, in this paper we shall focus on the kinematics around the generalized Kalnajcs discs, introduced by González & Reina (2006). They form an infinite family of axially symmetric finite thin discs, whose first member is precisely the well-known Kalnajcs disc (1972). The paper is organized as follows. First, in section 2, we present a summary of the main aspects of the generalized Kalnajcs discs, the surface densities, the gravitational potential and the motion equations. Then, in section 3 we shall focus on equatorial orbits, i.e. $z = 0$ trajectories ($\xi = 0$, $\eta = \sqrt{1 - R^2/a^2}$ inside the disc and $\xi = \sqrt{R^2/a^2 - 1}$, $\eta = 0$ outside). At first we shall study the stability under radial and vertical perturbations of circular orbits, then examining the principal features and conditions of general equatorial orbits. In the next section, section 4, we present numerical solutions of (7) describing some representative Poincaré surfaces of section. As it is expected, we find chaotic sections for disk-crossing orbits and regular sections for other cases. Some meridional plane orbits are plotted and the Lyapunov

* E-mail: javiramos1976@gmail.com

† E-mail: framsol@gmail.com

‡ E-mail: gonzalez@gag-girg-uis.net

characteristic numbers (LCN) are calculated. Finally, in section 5, we summarize our main results.

2 THE GENERALIZED KALNAJS DISCS

In this paper we shall focus on the kinematics around generalized Kalnajs discs, introduced by González & Reina (2006). They form an infinite family of axially symmetric finite thin discs, whose first member is precisely the well-known Kalnajs disc (1972). The mass surface density of each model (labeled with the positive integer m) is given by

$$\Sigma_m(R) = \frac{(2m+1)M}{2\pi a^2} \left[1 - \frac{R^2}{a^2}\right]^{m-1/2}, \quad (1)$$

where M is the total mass and a the disc radius. Such mass distribution generates an axially symmetric gravitational potential, that can be written in terms of Legendre polynomials P_n and second kind Legendre functions Q_n as

$$\Phi_m = - \sum_{n=0}^m C_{2n} P_{2n}(\eta) i^{2n+1} Q_{2n}(i\xi). \quad (2)$$

Here, $-1 \leq \eta \leq 1$ and $0 \leq \xi < \infty$ are spheroidal oblate coordinates, related to the usual cylindrical coordinates (R, z) through the relations

$$R^2 = a^2(1 + \xi^2)(1 - \eta^2), \quad z = a\eta\xi. \quad (3)$$

The constants C_{2n} appearing in (2) are given by

$$C_{2n} = \frac{MG}{2a} \left[\frac{\pi^{1/2}(4n+1)(2m+1)!}{2^{2m}(2n+1)(m-n)\Gamma(m+n+\frac{3}{2})q_{2n+1}(0)} \right],$$

where $q_{2n}(\xi) = i^{2n+1}Q_{2n}(i\xi)$ and G is the gravitational constant. Now, due to the presence of the term $(m-n)!$ at the denominator, all the C_{2n} constants vanish for $n > m$.

According to (2), the gravitational potentials corresponding to the first four members are given by

$$\Phi_1(\xi, \eta) = -\frac{MG}{a} [\cot^{-1} \xi + A(3\eta^2 - 1)], \quad (4a)$$

$$\begin{aligned} \Phi_2(\xi, \eta) = & -\frac{MG}{a} [\cot^{-1} \xi + \frac{10A}{7}(3\eta^2 - 1) \\ & + B(35\eta^4 - 30\eta^2 + 3)], \end{aligned} \quad (4b)$$

$$\begin{aligned} \Phi_3(\xi, \eta) = & -\frac{MG}{a} [\cot^{-1} \xi + \frac{5A}{3}(3\eta^2 - 1) \\ & + \frac{9B}{11}(35\eta^4 - 30\eta^2 + 3) \\ & + C(231\eta^6 - 315\eta^4 + 105\eta^2 - 5)], \end{aligned} \quad (4c)$$

$$\begin{aligned} \Phi_4(\xi, \eta) = & -\frac{MG}{a} [\cot^{-1} \xi + \frac{20A}{11}(3\eta^2 - 1) \\ & + \frac{162B}{143}(35\eta^4 - 30\eta^2 + 3) \\ & + \frac{4C}{11}(231\eta^6 - 315\eta^4 + 105\eta^2 - 5) \\ & + D(6435\eta^8 - 12012\eta^6 + 6930\eta^4 \\ & - 1260\eta^2 + 35)], \end{aligned} \quad (4d)$$

with

$$A = \frac{1}{4}[(3\xi^2 + 1)\cot^{-1} \xi - 3\xi], \quad (5a)$$

$$B = \frac{3}{448}[(35\xi^4 + 30\xi^2 + 3)\cot^{-1} \xi - 35\xi^3 - \frac{55}{3}\xi], \quad (5b)$$

$$\begin{aligned} C = & \frac{5}{8448}[(231\xi^6 + 315\xi^4 + 105\xi^2 + 5)\cot^{-1} \xi \\ & - 231\xi^5 - 238\xi^3 - \frac{231}{5}\xi], \end{aligned} \quad (5c)$$

$$\begin{aligned} D = & \frac{7}{2342912}[(6435\xi^8 + 12012\xi^6 + 6930\xi^4 \\ & + 1260\xi^2 + 35)\cot^{-1} \xi - 6435\xi^7 - 9867\xi^5 \\ & - 4213\xi^3 - \frac{15159\xi}{35}]. \end{aligned} \quad (5d)$$

We restrict our attention to these four members. The kinematics corresponding to the remaining models ($m \geq 5$) is easily inferred from the features characterizing $m = 1, 2, 3, 4$. In all the calculations concerning with such models we choose $a = M = G = 1$, without loss of generality.

Since each Φ_m is static and axially symmetric, the specific energy E and the specific axial angular momentum ℓ are conserved along the particle motion. This fact restricts such motion to a three dimensional subspace of the (R, z, V_R, V_z) phase space. By defining an effective potential $\tilde{\Phi}_m$ as

$$\tilde{\Phi}_m = \Phi_m + \frac{\ell^2}{2R^2}, \quad (6)$$

the motion will be determined by the equations (Binney & Tremaine 1987)

$$\dot{R} = V_R, \quad \dot{z} = V_z,$$

$$\dot{V}_R = -\frac{\partial \tilde{\Phi}_m}{\partial R}, \quad \dot{V}_z = -\frac{\partial \tilde{\Phi}_m}{\partial z}, \quad (7)$$

together with

$$E = \frac{1}{2}(V_R^2 + V_z^2) + \tilde{\Phi}_m. \quad (8)$$

3 EQUATORIAL ORBITS

The equilibrium points of the autonomous system (7) are $V_R = V_z = z = 0$, $R = R_c$, where R_c must satisfy the equation

$$\left(\frac{\partial \tilde{\Phi}_m}{\partial R}\right)_{(R_c, 0)} = -\frac{\ell^2}{R_c^3} + \left(\frac{\partial \Phi_m}{\partial R}\right)_{(R_c, 0)} = 0, \quad (9)$$

that is the condition for a circular orbit in the plane $z = 0$. In other words, the equilibrium points of (7) occur when the test particle describes equatorial circular orbits of radius R_c , specific axial angular momentum given by

$$\ell_c = \pm \sqrt{R_c^3 \left(\frac{\partial \Phi_m}{\partial R}\right)_{(R_c, 0)}}, \quad (10)$$

and specific energy

$$E = \tilde{\Phi}_m(R_c, 0), \quad (11)$$

where the subscript c in ℓ_c indicates that we are dealing with circular orbits.

In order to study the stability of these orbits under

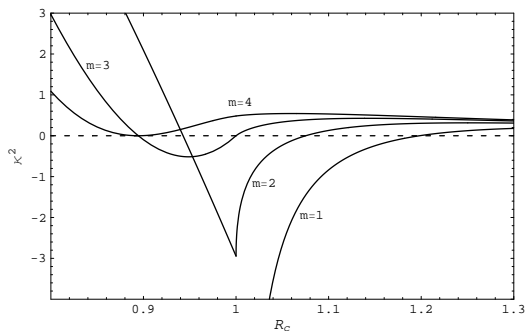


Figure 1. Behavior of κ^2 for $m = 1, 2, 3, 4$. Values of R_c such that this function is below the dashed line, corresponds to circular orbits that are unstable under radial perturbations.

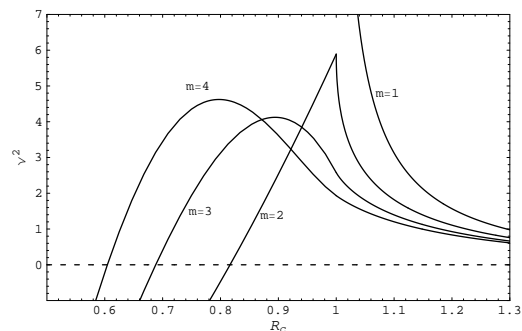


Figure 2. Behavior of ν^2 for $m = 1, 2, 3, 4$. Values of R_c such that this function is below the dashed line, corresponds to circular orbits that are unstable under vertical perturbations.

small radial and vertical (z -direction) perturbations, we analyze the nature of quasi-circular orbits. They are characterized by an epicycle frequency κ and a vertical frequency ν , given by (Binney & Tremaine 1987)

$$\kappa^2 = \left(\frac{\partial^2 \tilde{\Phi}_m}{\partial R^2} \right)_{(R_c, 0)}, \quad \nu^2 = \left(\frac{\partial^2 \tilde{\Phi}_m}{\partial z^2} \right)_{(R_c, 0)}. \quad (12)$$

This means that by introducing (10) in the second derivatives of $\tilde{\Phi}_m$ we obtain κ^2 and ν^2 as functions of R_c . Values of R_c such that $\kappa^2 > 0$ and (or) $\nu^2 > 0$ corresponds to stable circular orbits under small radial and (or) vertical perturbations, respectively. Otherwise we find unstable circular orbits. The case $m = 1$ presents radial stability in the range $0 \leq R_c \leq 1$ ($\kappa^2 = 3\pi$) but is radially unstable when $1 < R_c \leq 1.198$. For $m = 2$ and $m = 3$ we find radially unstable circular orbits with radius in the ranges $2\sqrt{2}/3 \leq R_c \leq 1.075$ and $2/\sqrt{5} \leq R_c \leq 1$, respectively. In contrast, circular orbits for $m = 4$ are always stable under small radial perturbations. We conjecture that models with $m \geq 5$ are also radially stable. Figure 1 shows the behavior of κ^2 as a function of R_c for $m = 1, 2, 3, 4$. Figure 2, showing the behavior of ν^2 , illustrates the stability under vertical perturbations. We find the following ranges of vertical instability: $0 \leq R_c \leq 1$ for $m = 1$ ($\kappa^2 = -3\pi/2$); $0 \leq R_c \leq 0.943$ for $m = 2$; $0 \leq R_c \leq 0.688$ for $m = 3$; $0 \leq R_c \leq 0.604$ for $m = 4$. We see that the range of vertical instability decreases with m .

General equatorial orbits are determined by (7) to-

gether with the conditions $\dot{V}_z = \dot{z} = z = 0$ and $E = V_R^2/2 + \tilde{\Phi}_m(R, 0)$. The motion is restricted by the inequality $E \geq \tilde{\Phi}_m(R, 0)$ and, in particular, we find bounded motion in a range $R_1 \leq R \leq R_2$ if it contains at least one critical value where $\tilde{\Phi}_m$ is minimum and $\tilde{\Phi}_m(R_1, 0) \leq E \leq \tilde{\Phi}_m(R_2, 0)$. Figure 3 shows the effective potential for $m = 2$ and $\ell = 1.242$, near the disc edge. At energies (a), (b), (c), and (d) we have bounded orbits, and (e), (f) corresponds to unbounded motion. In figure 4 we present the resulting phase portrait where the two regions of bounded and unbounded motion are divided by a separatrix curve (dashed line). Similar phase portraits can be performed for $m = 1$ and $m = 3$ if we set ℓ_c according to (10), for $1 < R_c \leq 1.198$ and $2/\sqrt{5} \leq R_c \leq 1$, respectively. For $m = 4$ the effective potential does not present local maximums and its phase portrait will not have any separatrix curve.

At a given energy E , determined by equation (11) once we fix R_c , the maximum possible value of the specific angular momentum is ℓ_c . Therefore, it is convenient to parameterize ℓ by means of the ratio $k = \ell/\ell_c$ (see next section). It is useful to calculate the range of values for ℓ_c such that $\tilde{\Phi}_m$ has a minimum in $0 \leq R \leq 1$, i.e. ensuring that bounded motion is always possible inside the disk. In this way, we establish the limiting values of the integrals of motion for which particles will never escape from the source. Using the relation (10), we found the following ranges for the specific axial angular momentum: (a) $m = 1$, $0 \leq |\ell_c| \leq \sqrt{3\pi}/2$; (b) $m = 2$, $0 \leq |\ell_c| \leq 2\sqrt{10\pi}/9$; (c) $m = 3$, $0 \leq |\ell_c| \leq \sqrt{21\pi}/50$; (d) $m = 4$, $0 \leq |\ell_c| \leq 15\sqrt{7\pi}/64$.

4 DISC-CROSSING ORBITS

In this section, we present numerical solutions of motion equations (7) corresponding to bounded orbits outside the equatorial plane (except when they cross the plane $z = 0$). For certain values of E and ℓ , they are confined to regions that contain the disc and will cross back and forth through it. As it was showed by Hunter (2005), this fact usually gives rise to many chaotic orbits due to the discontinuity in the z -component of the gravitational field, producing a fairly abrupt change in their curvatures. There is an important exceptional case of this behavior: the Kuzmin's disc, characterized by an integrable potential of the form $\Phi = -GM[R^2 + (a + |z|)^2]^{-1/2}$, with $a > 0$. However, the so-called Kuzmin-like potentials, characterized by $\Phi(\varepsilon)$ where $\varepsilon = [R^2 + (a + |z|)^2]^{1/2}$, are non-integrable and present the behavior mentioned above. Generalized Kalnajs models present a very similar structure and we can expect an analogous dynamics. Each potential $\tilde{\Phi}_m(\xi, \eta)$ can be cast in a Kuzmin-like form if we take into account that, according to (3), $\xi = (R_+ + R_-)/2a$ and $\eta = (R_+ - R_-)/2ia$, where $R_+ = [R^2 + (z + ia)^2]^{1/2}$ and $R_- = [R^2 + (z - ia)^2]^{1/2}$. Moreover, they are characterized by a z -derivative discontinuity in the disc, given by (González & Reina 2006)

$$\left(\frac{\partial \tilde{\Phi}_m}{\partial z} \right)_{z=0^+} = - \left(\frac{\partial \tilde{\Phi}_m}{\partial z} \right)_{z=0^-} = 2\pi G \Sigma_m(R). \quad (13)$$

Despite the above relation makes the KAM theorem inapplicable, we also found a large variety of regular disc-crossing orbits.

In Figure 5 we plot the level contours of $\tilde{\Phi}_m$ for $m =$

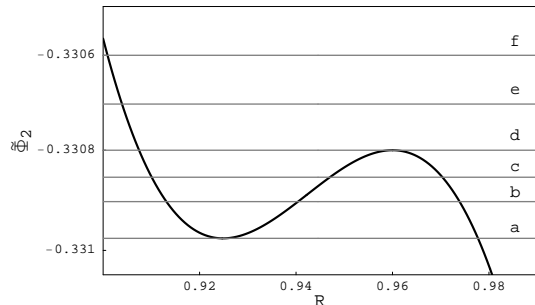


Figure 3. Effective potential for $m = 2$ and $\ell = 1.242$. Horizontal lines corresponds to the following specific energy values: (a) -0.330975 (minimum of $\tilde{\Phi}_2$), (b) -0.330900 , (c) -0.330850 , (d) -0.33079 (maximum of $\tilde{\Phi}_2$), (e) -0.330700 and (f) -0.330600 . Minimum and maximum of Φ_2 occur at $R_c = 0.925$ and $R_c = 0.960$.

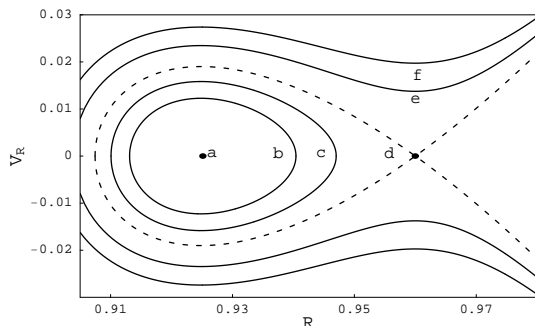


Figure 4. Phase portrait for $m = 2$, corresponding to the same values of ℓ and E showed in Figure 3. Here (a) and (d) are stable and unstable circular orbits, respectively. Curves (b) and (c) corresponds to stable bounded motion, while (b) and (f) describe unbounded motion. The dashed line represents a separatrix between bounded and unbounded motion regions.

1, 2, 3, 4, corresponding to $E = -1.245$ and $\ell = 0.2$, i.e. $k = 0.276, 0.266, 0.263$ and 0.262 , respectively. For this values, the motion of the particle is confined to a region containing the disc. The corresponding $z = 0$ surfaces of section are shown in Figs. 6-9, exhibiting a variety of regular and chaotic trajectories. The Fig. 6, that corresponds to the values determining the contour (a) in Fig. 5, shows a large KAM curve enclosing an island chain and three sets of three rings. There is also a stochastic region with two island chains near section's edge. The large KAM curve, the island chain and the central set of rings are produced by box orbits, while the lateral rings as well as the last two island chains are formed by loop orbits. The dotted curve, resulting from a banana boxlet periodic orbit, divide the regular and stochastic region.

Fig. 7 exhibits similar features as Fig. 6. This surface of section corresponds to the values defining the contour (b) shown in Fig. 5. In this case we see a defined central region of box orbits (four central rings) and an enclosing chaotic zone that contains a variety of resonant islands of loop orbits. In this case the regions of box and loop orbits are clearly separated, in contrast with Fig. 6 where they are alternated. The surface of section corresponding to $m = 3$ (contour (c) of Fig. 5) is showed in Fig. 8, exhibiting a regu-

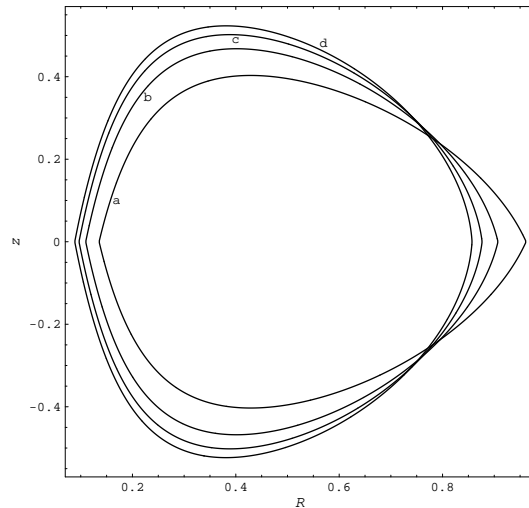


Figure 5. Level contours of (a) $\tilde{\Phi}_1$, (b) $\tilde{\Phi}_2$, (c) $\tilde{\Phi}_3$ and (d) $\tilde{\Phi}_4$, when $E = -1.245$ and $\ell = 0.2$.

m	$LCN(\pm 0.0001)$
1	0.0108
2	0.0110
3	0.0118
4	0.0120

Table 1. Estimation of the largest LCN for initial conditions $z = 10^{-10}$, $R = 0.681, V_R = 0.819$ of a disc-crossing orbit at the chaotic region of Figs. 6-9.

lar region composed by a central zone of banana boxlets and two resonant island chains of loops. In the chaotic region we see island chains again and three denser zones near the section's edge, formed by a loop orbit. Some of those meridional plane orbits are plotted in Fig. 10. Finally, Fig. 9 shows the surface of section for $m = 4$, $k = 0.262$ and $E = -1.245$. We find a very prominent chaotic region with only two island chains and a small regular region of box orbits.

The stochastic regions in Figs. 6-9 are due the overlapping of many resonances caused by presence of the disc (Hunter 2005). One can see this fact clearly in the three denser zones near the section's edge of Fig. 8, where the resonant islands are almost overlapped at $E = -1.245$. When the energy increases to -1.215 , for example, the overlapping is complete and the trajectory turns to be irregular (Fig. 11). In Fig. 9 we also note the footprint traced by the overlapping of three prominent central islands.

In order to quantify the degree of instability of the orbits we calculate their largest Lyapunov characteristic numbers (LCN), defined as

$$LCN = \lim_{\substack{\Delta_o \rightarrow 0 \\ t \rightarrow \infty}} \left[\frac{\ln(\Delta/\Delta_o)}{t} \right], \quad (14)$$

where Δ_o and Δ are the deviations of two orbits at times 0 and t respectively. We obtain LCN using the procedure of Benettin et al (1976). Thus by fixing the motion integrals

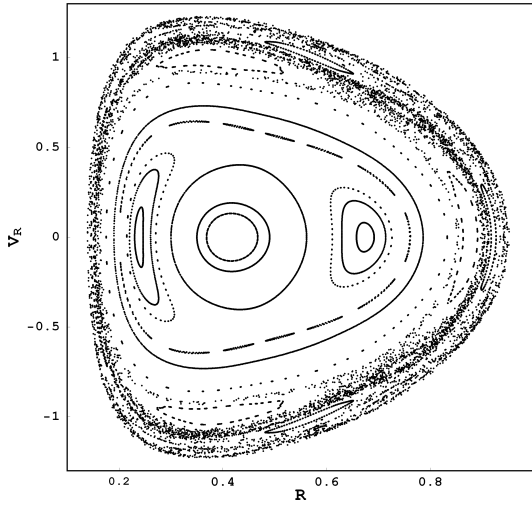


Figure 6. Surface of section for $m = 1$, $k = 0.276$ and $E = -1.245$. We have a small chaotic region with two resonant island chains and a central non-destroyed tori zone.

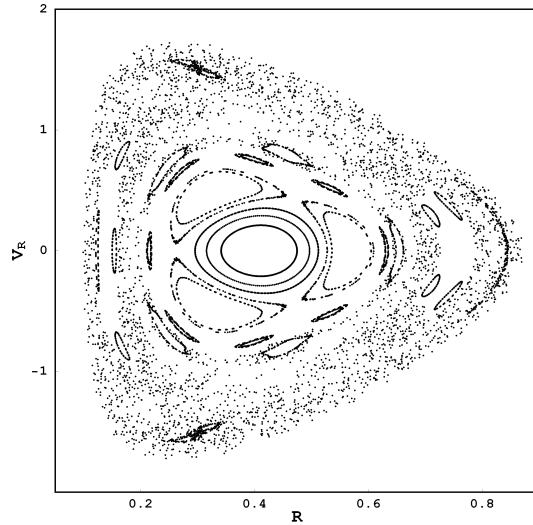


Figure 8. Surface of section for $m = 3$, $k = 0.263$ and $E = -1.245$. We see a prominent chaotic zone with island chains enclosing a regular region of box and loop orbits. The latter corresponds to the two central resonant islands.

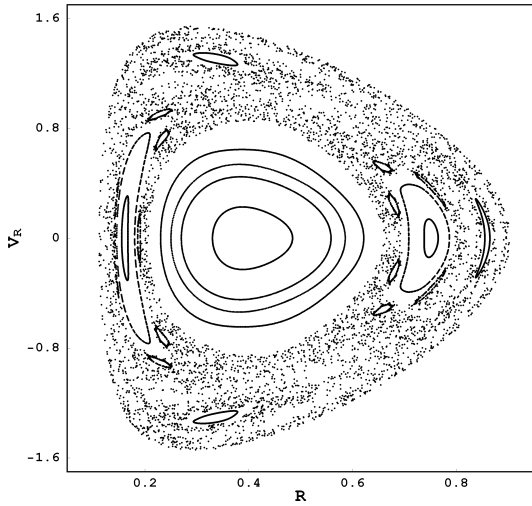


Figure 7. Surface of section for $m = 2$, $k = 0.266$, $E = -1.245$. The stochastic region is larger than in Fig. 6 and the non-destroyed tori zone is entirely formed by box orbits.

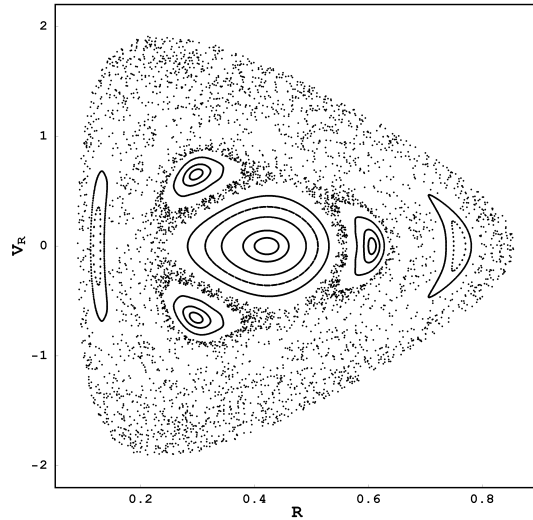


Figure 9. Surface of section for $m = 4$, $k = 0.262$ and $E = -1.245$. The chaotic region is larger than in the above figures and contain only two resonant island chains (the dotted curves at the extremum island are due to a periodic figure-of-eight orbit). The regular central zone is made entirely by box orbits.

as $E = -1.245$ and $\ell = 0.2$, choosing $\Delta_o \simeq 10^{-9}$ and $t = 10^7$, we estimate N corresponding to a typical chaotic disc-crossing orbit for the cases $m = 1, 2, 3, 4$ (Table 1). We found that the degree of instability increases modestly with m .

An interesting phenomenon occurs when the effective potential has saddle points outside the disc. This happens for the $m = 1$ and $m = 2$ discs, in whose case there are critical points in the ranges $1 < R_c \leq 1.198$ and $1 < R_c \leq 1.075$, respectively. Such equilibrium points are outside the disc but near its edge, so for certain values of E the contour of $\tilde{\Phi}_m$ will contain only a fraction of the disc and a $z = 0$ empty region. Then we will find bounded disc-crossing and non-disc-crossing orbits. For example, we choose $k = 0.673$ (corresponding to $R_c = 1.116$) and $E = -0.335$, obtaining the contour (a) of Fig. 12. The resulting surface of section

(Fig. 13) presents a large chaotic region to the left and a small totally regular region to the right. Both are divided by the saddle point, so for initial conditions near its left side the particle is “trapped” in the stochastic zone. In contrast, for initial conditions near the right side of the saddle point, the motion is confined to a region of non destroyed tori. In Fig. 14 we show a similar situation for $m = 2$. This surface of section corresponds to $k = 0.991$ ($R_c = 1.043$) and $E = -0.389$ (contour (b) of Fig. 12). We find a large zone of disc-crossing orbits with a small chaotic component enclosing an island chain and regular rings of banana boxlets. To the right of the saddle point there is a small regular region. For

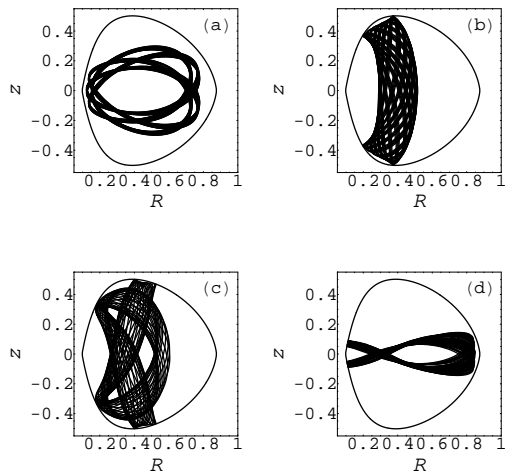


Figure 10. Orbits in the meridional plane for some initial conditions in Figure 8: (a) Loop orbit at $R = 0.739172$, $V_R = 0.362539$ (middle island chain inside stochastic region); (b) Banana boxlet orbit at $R = 0.421542$, $V_R = 0.362539$ (the largest central ring); (c) Pretzel shape loop orbit at $R = 0.405726$, $V_R = 0.573413$ (second island chain inside regular region); (d) A loop orbit at $R = 0.283155$, $V_R = 1.57197$ that forms the three denser zones near the section's edge. The outer boundary is the zero-velocity curve.

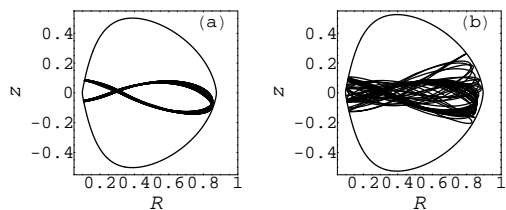


Figure 11. Orbits with the same ℓ and initial conditions as in Fig. 10 (d). In the case (a), where $E = -1.225$, the orbit is still regular, whereas it turns chaotic when $E = -1.215$ in case (b). The outer boundary is the zero-velocity curve.

the cases $m = 3$ and $m = 4$ it is not possible to obtain sections with the above features since their corresponding effective potentials have not saddle points (the product $\kappa^2 \nu^2$ is positive in $R > 1$).

5 CONCLUDING REMARKS

One remarkable fact, suggested by the analysis performed in Sect. 2, is that the stability of circular orbits under radial and vertical perturbations increases with the parameter m (for $m \geq 2$). More larger m corresponds to more stable models, when we deal with circular orbits. Another important fact is that the range of axial angular momentum for which we can find bounded motion inside the disc, decreases with m . Thus, loosely speaking, more and more stable models have less and less possibilities to maintain their particles

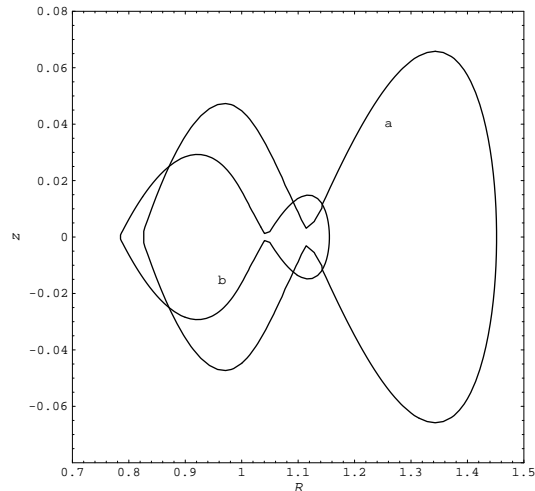


Figure 12. Level contours of (a) $\tilde{\Phi}_1$, $E = -0.335$, $\ell = 1.287$; (b) $\tilde{\Phi}_2$, $E = -0.389$, $\ell = 1.196$. Both cases have two connected regions, one of them containing the disc and the other is a disc-free zone.

inside the disc. These considerations have special relevance in the search of equilibrium distribution functions (they are E, ℓ -dependent) characterizing such galaxy models.

The numerical calculations showed in Sect. 3 confirm the analysis made by Hunter about disc-crossing orbits. There exist a chaotic motion induced by the presence of the disk and, despite the current versions of KAM theorem do not apply (due to the discontinuous force field), there is also a significant range of regular orbits. Moreover, since in our case we deal with finite disc models, a distinction between disc-crossing and non-disc-crossing orbits is sometimes necessary. In the latter case we did not find chaotic motion, even in extreme situations where there are saddle points outside the field source, and the disc and disc-free region are connected (Figures 13 and 14).

Although one would be tented to think that such hyperbolic exterior points can induce chaos at disc-free regions, what really happens is that the stochastic motion tends toward disc regions and a completely regular motion is developed outside there. These considerations have special relevance in galaxy models with thin disc plus halo components. Particles belonging to the halo component will follow a motion with the features mentioned above and, as it was showed by some authors, this fact determines decisively the internal structure of such stellar systems (see Ostriker, Spitzer and Chevalier (1972)).

6 ACKNOWLEDGMENTS

The authors thank to Leonardo Pachón for his valuable suggestions and orientations. G. A. G. and F. L-S. want to thank the financial support from COLCIENCIAS, Colombia, whereas that J. R-C. and F. L-S want to thank the financial support from *Vicerrectoría Académica*, Universidad Industrial de Santander.

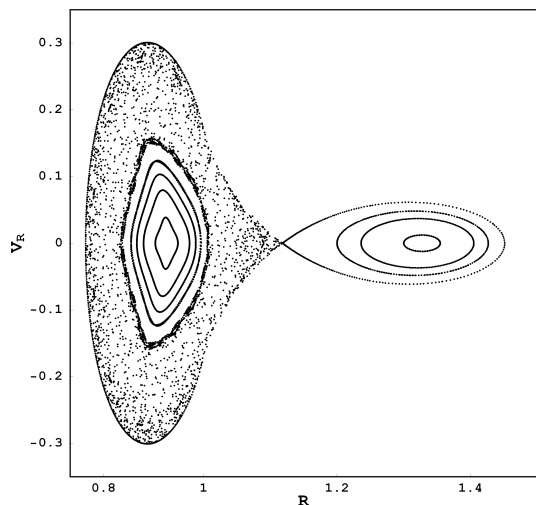


Figure 13. Surface of section for $m = 1$, $\ell = 1.287$ and $E = -0.335$ (contour (a) in Fig. 12). There is a prominent chaotic zone of disc-crossing orbits to the left of $R = 1.116$ (saddle point) and a regular region to the right.

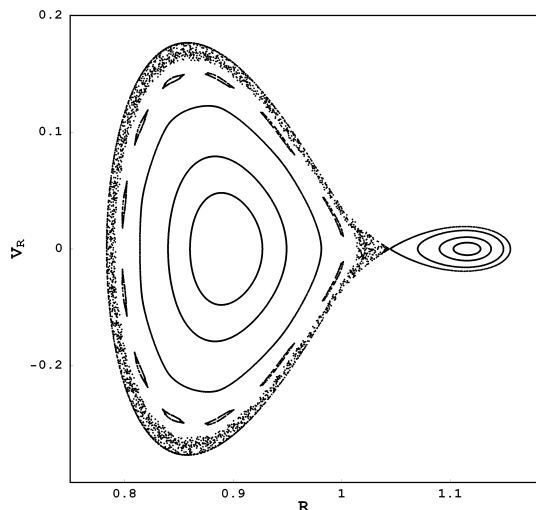


Figure 14. Surface of section for $m = 2$, $\ell = 1.196$ and $E = -0.389$ (contour (b) in Fig. 12). The disc-crossing region has a narrow stochastic zone and a prominent KAM-curves region. We have again a small regular zone to the left of saddle point at $R = 1.043$.

REFERENCES

- Benettin, G., Galgani, L. and Giorgilli A., 1972, Phys. Rev. A, 14, 2338.
 Binney, J. and Tremaine, S., 1987, Galactic Dynamics. Princeton University Press, Princeton, N. J.
 Brandt, J. C., 1960, Ap. J., 131, 211
 Brandt, J. C. and Belton, M. J. S., 1962, Ap. J., 136, 352
 González, G. and Reina, J. 2006, MNRAS, 371 (4), 1873-1876.
 Hunter, C., 1963, MNRAS, 126, 299
 Hunter, C., 2005, Ann. New York Acad. Sciences, 1045 (1),

- 120-138.
 Kalnajs, A. J., 1972, Ap. J., 175, 63.
 Kuzmin, G., 1956, Astron. Zh., 33, 27
 Martinet, L. and Hayli, A., 1971, A&A, 14, 103.
 Mayer, F. and Martinet, L., 1973, A&A, 27, 199.
 Martinet, L., 1974, A&A, 32, 329.
 Martinet, L. and Mayer, F., 1975, A&A, 44, 45.
 Ostriker, J. P., Spitzer, L., and Chevalier, R. A., 1972, ApJ, 176, L51.
 Schmidt, M., 1975, Bull. Astron. Inst. Neth, 13, 15.
 Toomre, A., 1963, Ap. J., 138, 385
 Toomre, A., 1964, Ap. J., 139, 1217
 Wyse, A. B. and Mayall, N. U., 1942, Ap. J., 95, 24